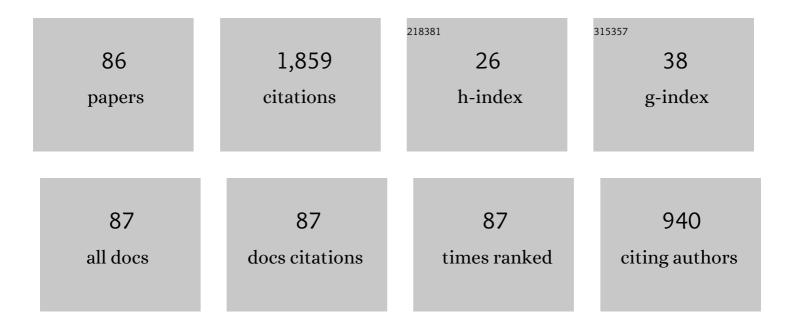
List of Publications by Year in descending order

Source: https://exaly.com/author-pdf/5195893/publications.pdf Version: 2024-02-01



#	Article	IF	CITATIONS
1	Effect of current on electrodeposited MnO2 as supercapacitor and lithium-ion battery electrode. Vacuum, 2022, 195, 110692.	1.6	14
2	Synergistic optimization of photothermoelectric performance of a perovkite/graphene composite. Ceramics International, 2022, 48, 4366-4370.	2.3	5
3	Optically tunable extrinsic chirality of single-layer metal metasurface for terahertz wave. Optics Communications, 2022, 512, 127554.	1.0	3
4	Improving performance of hybrid perovskite/graphene-based photodetector via hot carriers injection. Journal of Alloys and Compounds, 2022, 895, 162496.	2.8	10
5	Dynamic phase assembled terahertz metalens for reversible conversion between linear polarization and arbitrary circular polarization. Opto-Electronic Advances, 2022, 5, 210062-210062.	6.4	79
6	Reduced graphene oxide coated manganese dioxide electrode prepared by polyvinylpyrrolidone assisted electrodeposition. Vacuum, 2022, 199, 110925.	1.6	8
7	Manipulation of polarization conversion and multiplexing via all-silicon phase-modulated metasurfaces. Chinese Optics Letters, 2022, 20, 043601.	1.3	6
8	Terahertz metasurface zone plates with arbitrary polarizations to a fixed polarization conversion. , 2022, 1, 210014-210014.		42
9	Optically Tunable Terahertz Metasurface Absorber. Annalen Der Physik, 2022, 534, .	0.9	18
10	Resonance-trapped bound states in the continuum via all-silicon terahertz metasurface. Optics Communications, 2022, 516, 128274.	1.0	4
11	Excess polymer-assisted crystal growth method for high-performance perovskite photodetectors. Journal of Alloys and Compounds, 2022, 908, 164482.	2.8	9
12	Broadband and tunable terahertz absorption via photogenerated carriers in undoped silicon. Science China: Physics, Mechanics and Astronomy, 2022, 65, 1.	2.0	12
13	Inhibition of buried cavities and defects in metal halide perovskite photodetectors <i>via</i> a two-step spin-coating method. Journal of Materials Chemistry C, 2022, 10, 7886-7895.	2.7	13
14	Allâ€Dielectric Trifunctional Metasurface Capable of Independent Amplitude and Phase Modulation. Laser and Photonics Reviews, 2022, 16, .	4.4	36
15	Vector beam generation based on spin-decoupling metasurface zone plate. Applied Physics Letters, 2022, 120, .	1.5	6
16	A giantly chirality tunable terahertz metasurface based on 3D folded structure with vanadium dioxide. Optik, 2022, 262, 169305.	1.4	2
17	Dual-band giant spin-selective full-dimensional manipulation of graphene-based chiral meta-mirrors for terahertz waves. Optics Express, 2022, 30, 22292.	1.7	24
18	Versatile Polarization Conversion and Wavefront Shaping Based on Fully Phaseâ€Modulated Metasurface with Complex Amplitude Modulation. Advanced Optical Materials, 2022, 10, .	3.6	13

#	Article	IF	CITATIONS
19	Creating Longitudinally Varying Vector Vortex Beams with an Allâ€Dielectric Metasurface. Laser and Photonics Reviews, 2022, 16, .	4.4	43
20	Dynamic control of reflective chiral terahertz metasurface with a new application developing in full grayscale near field imaging. Carbon, 2021, 172, 189-199.	5.4	83
21	Ultrasonic and NH4+ assisted Ni foam substrate oxidation to achieve high performance MnO2 supercapacitor. Applied Surface Science, 2021, 541, 148546.	3.1	32
22	All-dielectric chiral coding metasurface based on spin-decoupling in terahertz band. Nanophotonics, 2021, 10, 1347-1355.	2.9	32
23	All-silicon metasurfaces for polarization multiplexed generation of terahertz photonic orbital angular momentum superposition states. Journal of Materials Chemistry C, 2021, 9, 5478-5485.	2.7	13
24	Fine manipulation of terahertz waves <i>via</i> all-silicon metasurfaces with an independent amplitude and phase. Nanoscale, 2021, 13, 5809-5816.	2.8	25
25	A dual band spin-selective transmission metasurface and its wavefront manipulation. Nanoscale, 2021, 13, 10898-10905.	2.8	19
26	Polarization-dependent and tunable absorption of terahertz waves based on anisotropic metasurfaces. Optics Express, 2021, 29, 3284.	1.7	24
27	Optically tunable all-silicon chiral metasurface in terahertz band. Applied Physics Letters, 2021, 118, .	1.5	41
28	Allâ€Dielectric Metasurface for Manipulating the Superpositions of Orbital Angular Momentum via Spinâ€Decoupling. Advanced Optical Materials, 2021, 9, 2002007.	3.6	44
29	Circular dichroism-like response of terahertz wave caused by phase manipulation via all-silicon metasurface. Photonics Research, 2021, 9, 567.	3.4	34
30	High energy storage MnO2@C fabricated by ultrasonic-assisted stepwise electrodeposition and vapor carbon coating. Chemical Engineering Journal Advances, 2021, 6, 100098.	2.4	7
31	Active controllable spin-selective terahertz asymmetric transmission based on all-silicon metasurfaces. Applied Physics Letters, 2021, 118, .	1.5	55
32	Multiple Longitudinal Polarization Vortices Generated via Allâ€&ilicon Metasurface. Annalen Der Physik, 2021, 533, 2100159.	0.9	3
33	Study on preparation of high performance manganese dioxide supercapacitor by cyclic voltammetry. Ionics, 2021, 27, 4521-4529.	1.2	3
34	Lossless dielectric metasurface with giant intrinsic chirality for terahertz wave. Optics Express, 2021, 29, 28329.	1.7	13
35	All-dielectric metasurfaces capable of dual-channel complex amplitude modulation. Nanophotonics, 2021, 10, 2959-2968.	2.9	10
36	All-silicon chiral metasurfaces and wavefront shaping assisted by interference. Science China: Physics, Mechanics and Astronomy, 2021, 64, 1.	2.0	18

#	Article	IF	CITATIONS
37	Terahertz wavefront shaping with multi-channel polarization conversion based on all-dielectric metasurface. Photonics Research, 2021, 9, 1939.	3.4	39
38	Free switch between bound states in the continuum (BIC) and quasi-BIC supported by graphene-metal terahertz metasurfaces. Carbon, 2021, 182, 506-515.	5.4	86
39	Multifunctional terahertz metasurfaces for polarization transformation and wavefront manipulation. Nanoscale, 2021, 13, 14490-14496.	2.8	20
40	Achiral Metasurfaces-Induced Circular Polarization Differential Transmittance. , 2021, , .		0
41	Dynamic conversion between bound states in the continuum (BIC) and quasi-BIC supported by terahertz metal metasurfaces. , 2021, , .		0
42	Spectral amplitude modulation and dynamic near-field displaying of all-silicon terahertz metasurfaces supporting bound states in the continuum. Applied Physics Letters, 2021, 119, .	1.5	46
43	Sodium Dodecylbenzene Sulfonate Assisted Electrodeposition of MnO ₂ @C Electrode for High Performance Supercapacitor. Journal of the Electrochemical Society, 2021, 168, 122502.	1.3	2
44	Significantly improved photoluminescence properties of ZnO thin films by lithium doping. Ceramics International, 2020, 46, 2309-2316.	2.3	76
45	High Specific Capacitance of the Electrodeposited MnO2 on Porous Foam Nickel Soaked in Alcohol and its Dependence on Precursor Concentration. Materials, 2020, 13, 181.	1.3	12
46	All-optical switchable terahertz spin-photonic devices based on vanadium dioxide integrated metasurfaces. Optics Communications, 2020, 460, 124986.	1.0	19
47	Highly Efficient Amplitude Modulation of Terahertz Fano Resonance Based on Si Photoactive Substrate by Low Power Continuous Wave. Advanced Materials Technologies, 2020, 5, 2000626.	3.0	19
48	Supercapacitor performances of MnO2 and MnO2/ reduced graphene oxide prepared with various electrodeposition time. Vacuum, 2020, 178, 109455.	1.6	48
49	Effective improvement of electrochemical performance of electrodeposited MnO2 and MnO2/reduced graphene oxide supercapacitor materials by alcohol pretreatment. Journal of Energy Storage, 2020, 30, 101511.	3.9	23
50	Metal-graphene hybrid active chiral metasurfaces for dynamic terahertz wavefront modulation and near field imaging. Carbon, 2020, 163, 34-42.	5.4	113
51	Photoresponse properties and energy gap of CsPbBr3–CsPb2Br5 compound thin film prepared by one-step thermal evaporation method. Journal of Materials Science: Materials in Electronics, 2020, 31, 4956-4962.	1.1	7
52	High performance MnO2 supercapacitor material prepared by modified electrodeposition method with different electrodeposition voltages. Journal of Energy Storage, 2020, 29, 101363.	3.9	65
53	Effects of electrodeposition time on a manganese dioxide supercapacitor. RSC Advances, 2020, 10, 15860-15869.	1.7	37
54	Graphene quantum dots doped ZnO superstructure (ZnO superstructure/GQDs) for weak UV intensity photodetector application. Ceramics International, 2020, 46, 17800-17808.	2.3	31

#	Article	IF	CITATIONS
55	Terahertz (THz) Generator and Detection. Electrical Science & Engineering, 2020, 2, .	0.2	8
56	Terahertz coding metasurface based vanadium dioxide. Wuli Xuebao/Acta Physica Sinica, 2020, 69, 228101.	0.2	5
57	Hybrid tunable chiral metasurfaces for amplitude and wavefront control of circularly polarized terahertz wave. , 2020, , .		0
58	High photoresponse sensitivity of lithium-doped ZnO (LZO) thin films for weak ultraviolet signal photodetector. Journal of Alloys and Compounds, 2019, 805, 309-317.	2.8	35
59	Co-effects of doping concentration and sintering temperature on structure and photoluminescence properties of sol-gel Y _{3â^'X} Ce _X Al ₅ O ₁₂ powder. Materials Research Express, 2019, 6, 086202.	0.8	1
60	Changes in the growth orientation, morphological and optical properties of sol-gel nanocrystalline ZnO thin films coated with different thickness. Materials Technology, 2019, 34, 80-85.	1.5	9
61	Surface nanosheets evolution and enhanced photoluminescence properties of Al-doped ZnO films induced by excessive doping concentration. Ceramics International, 2019, 45, 3871-3877.	2.3	35
62	Influence of oxygen vacancy on the response properties of TiO2 ultraviolet detectors. Journal of Alloys and Compounds, 2019, 779, 821-830.	2.8	30
63	Fabrication and characterization of dye-sensitized solar cells based on natural plants. Chemical Physics Letters, 2018, 693, 16-22.	1.2	34
64	Pretreating temperature controls on structural, morphological and optical properties of sol–gel ZnO thin films. Materials Technology, 2018, 33, 198-204.	1.5	9
65	Deposition time effects on optical gap, dark conductivity and X-ray photoresponse properties of thermal evaporated a-Se thin films. Journal of Materials Science: Materials in Electronics, 2018, 29, 19256-19263.	1.1	0
66	Evaporation time effects on structural, optical and X-ray photoresponse properties of thermal evaporated a-Se thin films at low vacuum degree. AIP Advances, 2018, 8, 095304.	0.6	1
67	Metal-insulator phase transition in Hf-doped VO ₂ (M) thin films: a study on the structural, electrical, optical and infrared radiation properties. Optical Materials Express, 2018, 8, 2300.	1.6	20
68	Hydrothermal preparation of ZnS: Mn quantum dots and the effects of reaction temperature on its structural and optical properties. Journal of Materials Science: Materials in Electronics, 2018, 29, 16715-16720.	1.1	15
69	Influence of sputtering power on structural, optical and electrical properties of CdTe thin films prepared by DC magnetron sputtering. Journal of Materials Science: Materials in Electronics, 2018, 29, 14635-14642.	1.1	10
70	Influence of Annealing Temperature on Structural, Morphological, Optical and Electrical Properties of Sol-Gel SnO ₂ Thin Films. Journal of Nano Research, 2018, 52, 15-20.	0.8	1
71	Investigations on Structural, Optical and X-Radiation Responsive Properties of a-Se Thin Films Fabricated by Thermal Evaporation Method at Low Vacuum Degree. Materials, 2018, 11, 368.	1.3	7
72	Influence of substrates on the properties of titanium nitride films deposited by DC reaction magnetron sputtering. Applied Physics A: Materials Science and Processing, 2018, 124, 1.	1.1	4

#	Article	IF	CITATIONS
73	Influence of substrate and Ar/N2 gas flow ratio on structural, optical and electrical properties of TiN thin films synthetized by DC magnetron sputtering. Journal of Materials Science: Materials in Electronics, 2018, 29, 9893-9900.	1.1	11
74	Performance of dye-sensitized solar cells based on natural dyes. Optical and Quantum Electronics, 2018, 50, 1.	1.5	9
75	Effect of the nitrogen–oxygen ratio on the position of N atoms in the TiO ₂ lattice of N-doped TiO ₂ thin films prepared by DC magnetron sputtering. CrystEngComm, 2018, 20, 4133-4140.	1.3	14
76	Structural and optical properties of nano-crystalline ZnO thin films synthesized by sol–gel method. Journal of Sol-Gel Science and Technology, 2017, 82, 563-568.	1.1	27
77	Regulations of aging time on optical properties of nano-crystalline ZnO thin films fabricated by sol–gel method. Functional Materials Letters, 2017, 10, 1750024.	0.7	0
78	Influence of electrolyte proportion on the performance of dye-sensitized solar cells. AIP Advances, 2017, 7, .	0.6	48
79	Annealing Temperature Dependence of Optical Properties of Sol-Gel ZnO Thin Films with Different Sol Aging Time. Journal of Nano Research, 2017, 48, 211-217.	0.8	3
80	Effects of aging time and annealing temperature on structural and optical properties of sol-gel ZnO thin films. AIP Advances, 2017, 7, 065213.	0.6	32
81	Influence of substrate on structural, morphological and optical properties of TiO2 thin films deposited by reaction magnetron sputtering. AIP Advances, 2017, 7, .	0.6	31
82	Substrate temperature effects on structural and photoelectric properties of CdS thin films. Surface Innovations, 2017, 5, 243-250.	1.4	4
83	Structural, Optical and Photoelectric Properties of Nano-Crystalline CdS Thin Films Deposited by Electron Beam Evaporation. Nanoscience and Nanotechnology Letters, 2017, 9, 1023-1027.	0.4	3
84	Enhanced Structural and Photoelectric Properties of CdCl ₂ Coated CdS Thin Films Deposited by Magnetron Sputtering. Nanoscience and Nanotechnology Letters, 2017, 9, 1363-1367.	0.4	2
85	Effect of Sn-Doped Concentration on Structural, Optical and Electrical Properties of ZnO:Sn (TZO) Thin Films Prepared by Sol–Gel Method. Nanoscience and Nanotechnology Letters, 2017, 9, 1539-1543.	0.4	1
86	Effects of annealing temperature on the structural and optical properties of ZnO thin films prepared by sol–gel method. Functional Materials Letters, 2016, 09, 1750010.	0.7	4